CDOM Absorption Properties of Natural Water Bodies along Extreme Environmental Gradients

Ciren Nima [1,*], **Øyvind Frette [2]**, **Børge Hamre [2]**, **Jakob J. Stamnes [2]**, **Yi-Chun Chen [2]**,
Kai Sørensen [3], **Marit Norli [3]**, **Daren Lu [4]**, **Qianguo Xing [5]**, **Dennis Muyimbwa [6]**,
Taddeo Ssenyonga [6], **Knut H. Stamnes [7]** and **Svein Rune Erga [8]**

[1]   Department of Physics, Tibet University, Lhasa 850000, China
[2]   Department of Physics and Technology, University of Bergen, 5020 Bergen, Norway;
      Oyvind.Frette@uib.no (Ø.F.); Borge.Hamre@uib.no (B.H.); Jakob.Stamnes@uib.no (J.J.S.);
      yi-chun.chen@uib.no (Y.-C.C.)
[3]   Norwegian Institute for Water Research, 0349 Oslo, Norway; kai.sorensen@niva.no (K.S.);
      Marit.Norli@niva.no (M.N.)
[4]   Institute of Atmospheric Physics, Chinese Academy of Sciences, Beijing 100029, China; ludr@mail.iap.ac.cn
[5]   Yantai Institute of Coastal Zone Research, Chinese Academy of Sciences, Yantai 264000, China;
      qgxing@yic.ac.cn
[6]   Department of Physics, Makerere University, Kampala 7062, Uganda; dmuyimbwa@cns.mak.ac.ug (D.M.);
      taddeo.ssenyonga@gmail.com (T.S.)
[7]   Stevens Institute of Technology, Hoboken, NJ 07030, USA; kstamnes@stevens.edu
[8]   Department of Biological Sciences, University of Bergen, 5020 Bergen, Norway; Svein.Erga@uib.no
*   Correspondence: crnmtu@163.com

Abstract: We present absorption properties of colored dissolved organic matter (CDOM) sampled in six different water bodies along extreme altitudinal, latitudinal, and trophic state gradients. Three sites are in Norway: the mesotrophic Lysefjord (LF), Samnangerfjord (SF), and Røst Coastal Water (RCW); two sites are in China: the oligotrophic Lake Namtso (LN) and the eutrophic Bohai Sea (BS); and one site is in Uganda: the eutrophic Lake Victoria (LV). The site locations ranged from equatorial to subarctic regions, and they included water types from oligotrophic to eutrophic and altitudes from 0 m to 4700 m. The mean CDOM absorption coefficients at 440 nm [$a_{CDOM}(440)$] and 320 nm [$a_{CDOM}(320)$] varied in the ranges 0.063–0.35 m^{-1} and 0.34–2.28 m^{-1}, respectively, with highest values in LV, Uganda and the lowest in the high-altitude LN, Tibet. The mean spectral slopes $S_{280-500}$ and $S_{350-500}$ were found to vary in the ranges of 0.017–0.032 nm^{-1} and 0.013–0.015 nm^{-1}, respectively. The highest mean value for $S_{280-500}$ as well as the lowest mean value for $S_{350-500}$ were found in LN. Scatter plots of $S_{280-500}$ versus $a_{CDOM}(440)$ and $a_{CDOM}(320)$ values ranges revealed a close connection between RCW, LF, and SF on one side, and BS and LV on the other side. CDOM seems to originate from terrestrial sources in LF, SF, BS, and LV, while RCW is characterized by autochthonous-oceanic CDOM, and LN by autochthonous CDOM. Photobleaching of CDOM is prominent in LN, demonstrated by absorption towards lower wavelengths in the UV spectrum. We conclude that high altitudes, implying high levels of UV radiation and oligotrophic water conditions are most important for making a significant change in CDOM absorption properties.

Keywords: CDOM absorption spectral slope; S$_R$; absorption coefficient; CDOM origin

1. Introduction

Colored (Chromophoric) dissolved organic matter (CDOM) refers to a complex group of organic compounds dissolved in natural water. It exists in all natural water bodies and absorbs light over a broad range of visible and ultraviolet (UV) wavelengths [1–4]. Over wide geographical areas, CDOM shows considerable differences in composition [1]. The sources of CDOM can be terrestrial inputs (allochtonous) or in situ (auotochthonous) due to phytoplankton [5], zooplankton [6], bacteria, and coral reefs.

Absorption properties of CDOM have been reported in numerous studies of marine water bodies [3,4,7–13]. CDOM absorption and dissolved organic carbon (DOC) concentration are closely connected in coastal water and lake water [14,15], but not in oceanic water, since there seems to be a decoupling between DOC and CDOM when dissolved organic matter (DOM) is transported offshore [16]. However, we did not measure DOC because we were mostly interested in the absorption properties of the colored component of DOC (i.e., CDOM) in the UV spectral region. DOC can not be measured optically, but is obtained by high temperature (catalytic) combustion (HTC). In general, for oceanic waters DOM is determined as DOC, which is the major element of organic matter, and consists mainly of low molecular weight compounds [17]. CDOM released from an individual source has distinct absorption peaks. For instance, CDOM production released from colonial cyanobacteria *Trichodesmium* sp. has absorption shoulders at about 325 nm and 360 nm [6], while CDOM released from a variety of zoo-plankton taxa has absorption peaks at wavelengths shorter than 300 nm [6].

Absorption of CDOM in the UV spectral region reduces both the level and penetration depth of the underwater UV radiation, and serves to protect underwater light-sensitive organisms from harmful UV radiation. Such protection is particularly critical for life in mountain lakes, since the UV radiation level increases with altitude [18,19] and mountain lakes often have lower CDOM concentrations than low-altitude lakes. However, exposure of CDOM to sunlight can lead to photo-bleaching and photo-induced degradation, which may result in reduced absorption of UV radiation and visible light [20–22] and increased penetration of harmful UV radiation in mountain lakes. Simultaneously, CDOM absorption in the visible spectral region reduces the availability of photosynthetically active radiation (PAR) for photosynthesis, and hence can contribute to reduced primary production [23] provided there are no other limiting factors, such as nutrients and grazing.

CDOM absorption in the visible spectral region is of interest in optical satellite remote sensing and to ocean optics researchers because CDOM is one of the major absorbing components in natural water [9]. Furthermore, the CDOM absorption spectrum, particularly in the blue spectral region, overlaps with that of chlorophyll and influences the accuracy of satellite-based estimation of Chl-*a* concentrations within the upper layer of the water column [24].

The absorption spectral slope S of CDOM can be used as an indicator to characterize CDOM in natural water bodies and to reveal their origin [25–27]. In general, S values are found to be higher in open oceanic water than in fresh water or coastal water [28]. S can be a useful indicator of changes in the composition of CDOM due to mixing of water bodies of different origins [29] or photo-bleaching [26]. Also, S is related to the average molecular weight of CDOM [26], bacterial production and abundance [30]. Stedmon et al. [31] and Matsuoka et al. [32] found an inverse relationship between the CDOM absorption coefficient at a certain wavelength and the CDOM spectral slope, whereas Vodacek et al. [33] and Babin et al. [10] did not find such a relationship. Helms et al. [26] found the spectral slope ratio S_R of $S_{275-295}$ to $S_{350-400}$ to be related to the molecular weight of dissolved organic matter and to photochemical induced shifts in molecular weight. Thus, upon light exposure of CDOM they found the percentage of CDOM in the low-molecular weight (LMW) (<1000 Da) fraction to increase, and the percentage in the high-molecular-weight (HMW) (>1000 Da) fraction to decrease, resulting in an increase of the S_R value. Conmy et al. [29] found changes in the CDOM absorption spectral slope $S_{280-312}$ with salinity to be a result of mixing of CDOM originating from freshwater and marine humics together with photo-bleaching in coastal water. Song et al. [34] discovered that the humic-like materials in CDOM tended to decrease with altitude in lakes.

For a specific water body, *S* values tend to be restricted to a narrow range [7,35]. However, when comparing slope values from different publications, one often finds large differences. A number of studies [28,36] have stressed that a direct comparison of optical properties of CDOM in different publications often is difficult due to methodological differences. To a certain degree, the application of different methods (i.e., the choice of wavelength interval for fitting, as well as the fitting method) obscures the true variability of the CDOM absorption spectral slope found in natural water bodies, and thus the variability in the composition of CDOM. Therefore, to obtain comparable and reliable data from large geographical areas, the same method should be used.

Previous studies on CDOM absorption properties for natural water bodies have been carried out in restricted areas and with differences in the methods used [10,32,37]. Thus, few studies have been conducted to study CDOM samples from areas with large differences in latitude, altitude, and trophic state, and by using the same method (i.e., the choice of wavelength interval for fitting as well as the fitting method). In the present study, we aimed at improving our knowledge on CDOM absorption properties for a wide range of water types, ranging from limnic to marine, and representing extreme gradients both in environmental conditions and geographical location. We believe this may provide new insights which are useful not only for a better understanding of CDOM dynamics, but also for application to ocean color remote sensing.

2. Data and Methods

2.1. Study Sites

In this study, we analyzed and compared absorption properties of 303 CDOM samples from six different water bodies, including two lakes, two fjords, and two coastal water bodies, having wide differences in optical properties, environmental conditions, and trophic state. These are: mesotrophic coastal-oceanic water around the island of Røst, Northern Norway (RCW), mesotrophic water of two western Norwegian fjords; the Samnangerfjord (SF) and the Lysefjord (LF), heavily polluted and eutrophic marine and limnic water; the Bohai Sea, China (BS), and Lake Victoria, Uganda (LV), and finally the oligotrophic high-altitude Lake Namtso, Tibet (LN). The locations of these six study sites are shown in Figure 1, and more information of each study site is given in Table 1. Their locations are as follows: (1) RCW, (2) SF, and (3) LF are at latitudes between 59 and 68° N and longitudes between 4 and 14° E in Norway; (4) BS and (5) LN are at latitudes between 30 and 41° N and longitudes between 90 and 122° E in China; and (6) LV is located close to the equator at latitudes between 0°30′ N and 2°30′ S and longitudes between 31°50′ E and 34°10′ E [38]. LN, which is situated on the Tibetan Plateau (TP) at 4718 m above sea level, has low contents of biota because of harsh environmental conditions with a short growing season (normally from mid-May until mid-September [39]), low temperatures (average annual temperature of −0.16 °C [40]), and high UV exposure (UV index values above 15 on the TP [41]). The BS and LV study sites are close to big cities, implying that large amounts of wastewater from industry and sewage discharge into these two water bodies lead to high levels of nutrients. At the shallow sampling stations (7–9 m) in LV the water column was homogenously mixed with respect to temperature, nutrients, CDOM, and Chl-*a* [42]. Therefore, surface samples are representative for all depths for these parameters. The SF and LF represent side branches of extensive fjord systems, which again have good connections with coastal water and the North Sea to the west. The fjords are the main input sources of freshwater to the Norwegian Coastal Current (NCC), and they are therefore characterized by distinct stratification of the upper water column and estuarine circulation [43]. RCW is strongly influenced by NCC and Atlantic water, and is located just above the Arctic Circle. In this water body, the Northeast Arctic cod, representing the strongest cod stock in the world, comes in for spawning in March–April [44], making this area particularly important for fisheries and vulnerable to environmental threats. Due to few and variable sampling times at the various sites during the year, and the fact that LV, which is situated close to the Equator, has small seasonal variations, we decided not to include seasonal variations in our analysis.

Table 1. For each study site, the columns show sampling periods, depths, number of samples, water type, Chl-*a* concentration, euphotic depth, trophic state and the vertical diffuse attenuation coefficient for photosynthetically active radiation (PAR). Capitalized letters in parentheses in the first column are abbreviations for the study sites. The symbols '0', 'hs', and 's' in the third column refer to measurements at the surface, at half the Secchi depth, and at the full Secchi depth, respectively. Euphotic depth is the depth at which PAR falls to 1% of its subsurface value. Trophic state: OT for oligotrophic, MT for mesotrophic and ET for eutrophic.

Study Site	Sampling Periods	Depths [m]	Number of Samples	Water Type	Chl-*a* [μgL^{-1}]	Euphotic Depth [m]	Trophic State	K_d(PAR) [m^{-1}]
Samnangerfjord	March 1999	0, 10, 50	85	fjord	0.01–6.3 [11]	12–38	MT	0.12–0.4 *
(SF)	October 1999							
	January 2000							
Lake Victoria	October 2003	surface	8	lake	4.8–60.7 [35]	2–2.4	ET	1.93–2.25 [42]
(LV)	November 2003							
	December 2003							
	January 2004							
Lysefjord	January 2011	1, 10, 25, 50	29	fjord	0.5–5 [43]	12–35	MT	0.13–0.38 [43]
(LF)								
Bohai Sea	September 2012	0, hs, s	36	coastal	0.97–8.80	6–16	ET	0.29–0.72 **
(BS)	September 2013							
	August 2014							
Lake Namtso	July 2013	0, hs, s	36	lake	0.01–0.17 [45]	29–38	OT	0.12–0.16
(LN)	August 2014							
Røst Coastal Water	May 2013	0, hs, s	109	coastal	0.17–1.94 [46]	26–51	MT	0.09–0.18 ***
(RCW)	October 2013							
	April 2014							
	October 2014							
	March 2015							
Total			303					

* Values representative for maximum water column Chl-*a* concentrations from 0.2–6 [μgL^{-1}](unpubl. data). ** BS-Yellow River: K_d(PAR) > 1.8 [m^{-1}] (this study). *** Jan Mayen Front in the Norwegian Sea (westwards from Røst): Chl-*a* = 0.2–3.5 [μgL^{-1}], K_d(400–600 nm) = 0.07–0.30 [m^{-1}], K_d(380 nm) = 0.13–0.20 [m^{-1}], K_d(465 nm) = 0.08–0.17 [m^{-1}] [47].
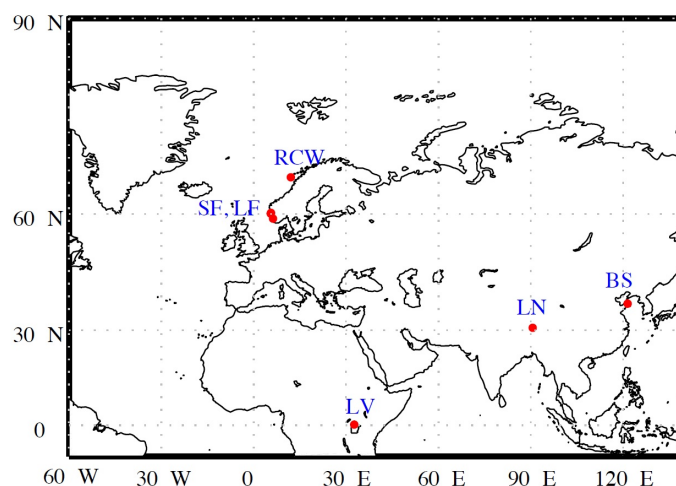
Figure 1. World map with solid red dots indicating the six study sites: LV = Lake Victoria, Uganda; LN = Lake Namtso, Tibet; BS = Bohai Sea, China; SF = Samnangerfjord, Norway, LF = Lysefjord, Norway; RCW = Røst Coastal Water, Norway.

2.2. Determination of CDOM Absorption Coefficient and Spectral Slope

Samples collected from SF and LF (Table 1) were analyzed as follows. Water samples were filtered through a 0.2 µm Nucleopore filter and stored in opaque glass bottles at 4 °C for a few days before analysis in the laboratory. CDOM absorbance spectra were measured at wavelengths within the interval between 250 and 650 nm with 2 nm increments using a 10 cm quartz cuvette and a Shimadzu MPS 2000 spectrometer [11]. The detection limit for abs in the Shimadzu MPS 2000 spectrophotometer is ±0.003.

Water samples collected from LV (Table 1) were filtered through a Nucleopore membrane filters with 0.2 µm pore size and the CDOM samples were stored in acid cleaned glass bottles in a refrigerator until analysis. The CDOM absorption was determined for wavelengths between 200 and 900 nm using a dual-beam Perkin Elmer Lambda 40P spectrophotometer at the Norwegian Institute for Water Research (NIVA). The measurements were performed relative to distilled water [35].

Samples collected from LN, BS, and RCW (Table 1) were analyzed as follows. Water samples were filtered through Whatman Polycarbonate filters (diameter 47 mm, pore size 0.22 µm) at low vacuum pressure on the day they were collected, and the filtrate was collected in pre-washed bottles. The bottles were pre-rinsed three times with filtered sample water to minimize the possibility of contamination. At some locations and depths, duplicate samples were prepared. The CDOM samples were stored in a dark refrigerator until analysis. Such preparation and storage of CDOM samples have been shown to be sufficient for avoiding microbial degradation for more than five months [48,49]. Prior to analysis, the CDOM samples and Milli-Q water were acclimated to room temperature. The absorbance spectra were recorded at wavelengths in the range from 200 to 900 nm with 2 nm increments using a dual-beam Shimadzu spectrophotometer (UV-1800) equipped with a 10 cm quartz cuvette. The detection limit for abs in the Shimadzu spectrophotometer (UV-1800) is ±0.008. Baseline data were obtained by filling Milli-Q water both in the sample and reference cells, and baseline correction was obtained by subtracting the offset from each sample spectrum.

All measured absorbance data were converted into absorption coefficients using

$$a_{\mathrm{CDOM,m}}(\lambda) = 2.303 \times A(\lambda)/\ell, \tag{1}$$

where the subscript 'm' stands for measured, and where $a_{\mathrm{CDOM,m}}(\lambda)$ and $A(\lambda)$ are the measured absorption coefficient [m^{-1}] and absorbance, respectively, at wavelength λ, and ℓ is the path length in [m] ($\ell = 0.1$ m). In Equation (1), the number 2.303 is the conversion factor between the base 10 logarithm and the natural logarithm. The absorption coefficient for CDOM generally exhibits a

behaviour according to which it decreases approximately exponentially with increasing wavelength in the near-UV and visible spectral regions, i.e., (Bricaud et al. [7])

$$a_{\text{CDOM}}(\lambda) = a_{\text{CDOM}}(\lambda_0) \exp[-S(\lambda - \lambda_0)]. \tag{2}$$

Here $a_{\text{CDOM}}(\lambda)$ and $a_{\text{CDOM}}(\lambda_0)$ are the absorption coefficients at the wavelength of observation λ and a reference wavelength λ_0, respectively. The absorption coefficient $a_{\text{CDOM}}(\lambda_0)$ is used to characterize the CDOM concentration in a specific water body, and the spectral slope S [nm^{-1}], which is independent of λ_0, indicates how rapidly the absorption decreases with increasing wavelength. The absorption coefficient of CDOM at 440 nm is commonly used to characterize the CDOM concentration (see Table 3.2 in Kirk [1]), since this wavelength corresponds approximately to the mid-point of the blue waveband peak that most classes of algae have in their photosynthetic action spectra [1]. In water bodies where the CDOM absorption is low at longer wavelengths, the absorption coefficient can be measured in the near-UV spectral range (350–400 nm) with higher absorption, and a_{CDOM}(440 nm) can then be estimated using Equation (2). In these cases the absorption coefficients at 355 or 375 nm are preferred [15].

To correct for scattering due to residual particles (<0.22 μm) in CDOM samples, we used a method similar to that of Babin et al. [10] and Matsuoka et al. [32], according to which the measured CDOM absorption coefficient is corrected for scattering due to residual particles at all spectral values by subtracting the measured absorption coefficient averaged over a 5-nm interval around 685 nm. For the samples collected from SF the absorption spectra were measured between 250 and 650 nm [11], hence no scattering correction was performed.

After correction for scattering, two commonly used fitting methods [7,10,11], referred to as the linear fitting method and the nonlinear fitting method, were applied to all CDOM data to determine the CDOM absorption spectral slope S. The linear fitting method is based on fitting the natural logarithm of the measured CDOM absorption spectrum to a natural logarithm transformation of Equation (2), whereas the nonlinear fitting method is based on directly fitting the measured CDOM absorption spectrum to Equation (2). The CDOM absorption spectral slope S depends on the wavelength interval used for deriving it [9,36]. Therefore, we derived the spectral slope by fitting the measured absorption coefficients in two different wavelength intervals, i.e., 280–500 and 350–500 nm to Equation (2) using both the linear and the nonlinear fitting method. The S values derived using these two wavelength intervals are denoted $S_{280-500}$ and $S_{350-500}$. A comparison of the CDOM spectral slopes derived by applying these two methods over the wavelength intervals 350–500 nm ($S_{350-500}$) and 280–500 nm ($S_{280-500}$) (data not shown), revealed that the $S_{350-500}$ derived by applying nonlinear and linear fitting agree quite well, but with slightly higher values obtained from nonlinear fitting. A comparison of the spectral slope S derived for the 412–650 nm interval by Twardowski et al. [36] and the 350–500 nm interval by Stedmon et al. [8] shows a similar agreement. However, as the wavelength interval used for fitting is further extended to wavelengths shorter than 350 nm, i.e., to obtain $S_{280-500}$, the disparity between the values derived from these two methods becomes large; indicating that the spectral slope S derived for a wavelength interval including the short UV spectral region tends to be strongly affected by the fitting method. Therefore, clarification of the fitting method becomes particularly important for a water body such as LN in this study, which is exposed to high UV radiation levels and has a modest supply of CDOM from its catchment areas. Based on our testing, and in agreement with Stedmon et al. [8], Blough and Del Vecchio [28], and Granskog et al. [50], we found it best to apply nonlinear fitting to our data. To obtain the slope ratio S_R, we first used nonlinear fitting to derive $S_{280-295}$ and $S_{350-400}$, and then we calculated S_R as $S_R = S_{280-295}/S_{350-400}$.

2.3. Determination of Chl-a Concentration

In [46] a detailed description is given of how to determine the Chl-*a* concentration. A brief summary is as follows. Water samples were filtered on the day of collection, and sample filters were

stored in a freezer with dry ice before and during transportation. Next, all samples were stored in a freezer at $-78\,^\circ$C or $-80\,^\circ$C. Both high pressure liquid chromatography (HPLC) and spectrophotometry were used to determine the Chl-*a* concentrations. For details, see [46].

2.4. Determination of the Vertical Diffuse Attenuation Coefficient for the Downward Irradiance K_d

The K_d(PAR) values shown in Table 1 for LN, BS, and RCW were calculated using the relationship $K_d = 1.44/Z_{SD}$ derived by Holmes [51], where Z_{SD} is the Secchi disk depth and K_d is the vertical diffuse attenuation coefficient for the downward irradiance. For SF, LF, and LV, K_d(PAR) values were calculated from 400–700 nm PAR sensor measurements between the surface and the lower part of the euphotic zone.

3. Results and Discussion

3.1. CDOM Absorption Characteristics of Different Water Types

Figure 2 shows the mean CDOM absorption spectrum for each study site obtained by averaging over all samples. Among the six study sites, the highest mean absorption coefficients for the wavelength range 280–500 nm were found in LV and the second highest values in BS. These two water bodies receive high amounts of water discharges from industry, agriculture, aquaculture, and sewage and often have high concentrations of organic matter, which, as shown in Table 1, are associated with extremely high concentrations of Chl-*a* in LV, low penetration of PAR indicated by K_d(PAR) and shallow euphotic zone. It follows from Figure 2 that the mean CDOM absorption spectra for samples from SF and LF in western Norway were quite similar, but higher than those from RCW. However, it should be noted that maximum Chl-*a* concentrations around 2–10 times our value for RCW have been found during spring bloom in other years in many fjords of Northern Norway, including Vestfjorden, which is adjacent to RCW [52]. Further, LN on the TP had the lowest mean values of CDOM absorption, which can be attributed to a combination of low contents of organic matter, which is typical for high-altitude lakes, a high level of photo-bleaching resulting from high UV radiation levels on the TP [53,54], and a long water retention time due to the lack of outflow rivers [45]. The CDOM absorption is reduced upon exposure to sunlight [20–22], and the rate of photo-bleaching differs between spectral regions [22,55]. From Figure 2b, which shows semi-log plots of the CDOM spectra in Figure 2a, it can be seen that the mean absorption spectrum for LN has inflection points and approximately exponential behavior over short discrete wavelength intervals. Similar absorption spectra have been found for CDOM samples obtained from the deep ocean or from surface water after photo-bleaching [9]. It is known that mycospirine-like amino acids (MAAs), which absorb within the range 309–360 nm [56], are present in many diverse environments, and therefore could contribute to the CDOM absorption [57,58]. In our data there is a weak bump in the CDOM absorption spectra for LN around 340 nm (Figure 2), which may indicate the presence of MAAs.

As shown in Table 2, the measured mean CDOM absorption coefficients for LV and BS were found to be respectively 2.28 and 1.96 m^{-1} at 320 nm, and 0.35 and 0.29 m^{-1} at 440 nm. They were much higher than the corresponding values found in RCW and LN, for which the values were respectively 0.73 and 0.34 m^{-1} for $a_{\mathrm{CDOM}}(320)$, and 0.11 and 0.063 m^{-1} for $a_{\mathrm{CDOM}}(440)$. Still none of our $a_{\mathrm{CDOM}}(440)$ water values are as high as those in Chinese rivers, which have mean values within the range 0.6–2.4 m^{-1} [59,60]. On the other hand, the absorption properties of our marine water bodies (Table 2) seem to be consistent with those of the Arctic Ocean, where $a_{\mathrm{CDOM}}(440)$ values are typically <0.5 m^{-1} [32], and $a_{\mathrm{CDOM}}(375)$ values $\leq$0.73 m^{-1} [61]. Among the marine study sites, salinity varied between 10–34 and 15–33, respectively, in SF and LF for the depth interval 0–30 m [11,43]. Monitoring of coastal water around Røst (Institute of Marine Research) at the times of our samplings shows salinity values in the range 30.1–33.4 for the depth interval 1–30 m (http: //www.creativecommons.no/), while typical salinities for surface and bottom water of BS are within the range 24–31.5 [62]. The tendency of an inverse relationship between CDOM absorption and salinity

can be seen at our near shore stations (SF, LF, and BS), which are strongly influenced by freshwater outlets, and this tendency is in accordance with Aksnes et al. [63], who concluded that Norwegian coastal water has "darkened" due to freshening during the period 1935–2007.

Table 2. The maximum (max), minimum (min), mean, and standard deviation (STD) values for the measured colored dissolved organic matter (CDOM) absorption coefficients at 320 nm [$a_{CDOM}(320)$], 325 nm [$a_{CDOM}(325)$], 355 nm [$a_{CDOM}(355)$], 375 nm [$a_{CDOM}(375)$], 412 nm [$a_{CDOM}(412)$], and 440 nm [$a_{CDOM}(440)$] at each study site.

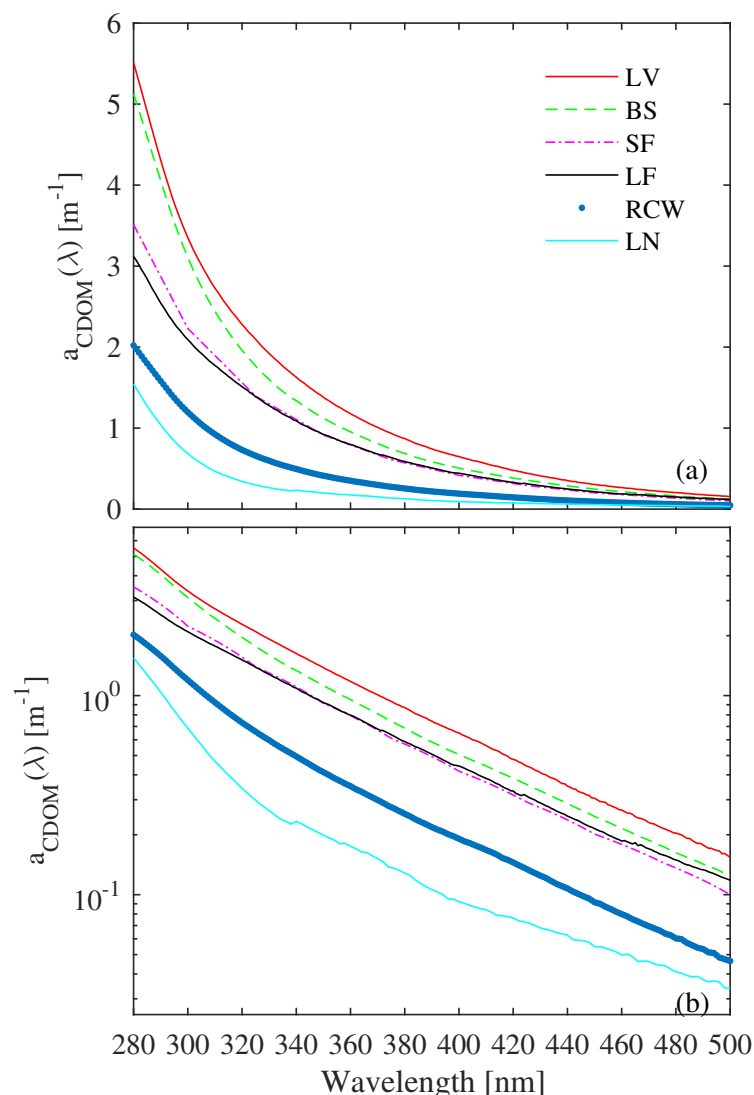| Absorption Coefficient [m^{-1}]	Location	Max [m^{-1}]	Min [m^{-1}]	Mean [m^{-1}]	STD [m^{-1}]
$a_{CDOM}(320)$	LV	2.95	1.69	2.28	0.53
	LN	0.94	0.22	0.34	0.12
	BS	3.72	1.33	1.96	0.59
	RCW	1.35	0.48	0.73	0.16
	LF	2.51	0.67	1.51	0.63
	SF	4.43	0.54	1.56	0.67
$a_{CDOM}(325)$	LV	2.71	1.53	2.10	0.49
	LN	0.77	0.19	0.30	0.10
	BS	3.37	1.20	1.77	0.51
	RCW	1.24	0.44	0.66	0.15
	LF	2.30	0.61	1.39	0.57
	SF	4.08	0.48	1.40	0.61
$a_{CDOM}(355)$	LV	1.64	0.91	1.27	0.31
	LN	0.31	0.09	0.18	0.05
	BS	2.14	0.76	1.03	0.26
	RCW	0.80	0.24	0.38	0.10
	LF	1.39	0.39	0.86	0.34
	SF	2.60	0.30	0.85	0.38
$a_{CDOM}(375)$	LV	1.20	0.67	0.94	0.22
	LN	0.22	0.06	0.14	0.04
	BS	1.58	0.56	0.74	0.19
	RCW	0.63	0.18	0.28	0.08
	LF	1.04	0.30	0.64	0.25
	SF	1.86	0.22	0.61	0.28
$a_{CDOM}(412)$	LV	0.68	0.38	0.54	0.12
	LN	0.12	0.03	0.08	0.02
	BS	0.99	0.31	0.43	0.12
	RCW	0.43	0.10	0.16	0.06
	LF	0.61	0.18	0.37	0.13
	SF	1.07	0.10	0.36	0.16
$a_{CDOM}(440)$	LV	0.44	0.24	0.35	0.08
	LN	0.092	0.023	0.063	0.017
	BS	0.73	0.22	0.29	0.09
	RCW	0.32	0.055	0.11	0.05
	LF	0.40	0.11	0.25	0.09
	SF	0.71	0.05	0.24	0.11

Figure 2. (**a**) Mean colored dissolved organic matter (CDOM) absorption spectra for different locations. (**b**) Semi-log plots of the CDOM absorption spectra in (**a**).

Comparison of our mean value for $a_{CDOM}(355)$ (1.27 m^{-1}) in the eutrophic LV with mean values for $a_{CDOM}(350)$ in Chinese eutrophic lakes, which varies between 2.75 and 4.57 m^{-1} [64,65], shows that CDOM concentrations in LV are lower, even though the Chl-*a* concentrations are at the same level. The trophic state of an aquatic system can be described in terms of concentrations of the dissolved nutrients nitrogen and phosphorus. When the concentrations of these nutrients are low (oligotrophic), they limit algal growth, and when they are high (eutrophic), they trigger algal growth, resulting in respectively low and high concentrations of total phosphorus (TP) and Chl-*a*, and large and small Secchi depths, respectively [65]. For lakes in China, typical $a_{CDOM}(355)$ mean values for oligotrophic, mesotrophic (medium level of nutrients), and eutrophic water bodies are 1.47, 2.75, and 4.21 m^{-1}, respectively [15]. For coastal water of the Baltic Sea, $a_{CDOM}(375)$ values are within the range 0.41–7.92 m^{-1}, with a mean value of 1.61 m^{-1} [66]. This is much higher than our mean value for $a_{CDOM}(375)$ in Norwegian coastal water (Table 2), actually six times higher than in RCW and 2.5 times higher than in SF and LF. For coastal water of Hudson Bay, Granskog et al. [50] give an $a_{CDOM}(355)$ average of 1.81 m^{-1}, which is more than two times higher than our average of 0.85 m^{-1} for fjord water. In a trophic state perspective (see definitions above of oligotrophic, mesotrophic, and eutrophic), the use of CDOM

absorption properties to classify water bodies does not seem to be appropriate in our case, since even LV will fall into the category oligotrophic ($a_{CDOM}(355) = 1.27 \text{ m}^{-1}$) and so will Norwegian fjords.

3.2. Using Absorption Spectral Slope to Uncover CDOM Origins

Several authors [8,32,36] have pointed out that the CDOM absorption spectral slope S depends on the wavelength interval used for fitting, which is also confirmed by our data. Thus, scatter plots of the spectral slopes derived for the wavelength intervals 280–500 nm versus 350–500 nm show that the values of $S_{280-500}$ are generally higher than the values of $S_{350-500}$ for all water bodies (Figure 3). It can also be seen that all S values for the different water bodies are closely connected, except for the S value for LN. The reason why the CDOM absorption coefficients for LN water samples consistently are separated from those for the other water bodies, as revealed by high $S_{280-500}$ values in Figure 3, could be due to the fact that LN is a high-altitude mountain lake with very low levels of high molecular CDOM in the freshwater inlets. This is probably a consequence of extreme environmental conditions, characterized by a poorly developed soil and vegetation, and high UV radiation levels because of increased solar radiation with altitude [18,19], and the existence of a low total ozone column during summer [67]. Therefore as shown in Table 3, LN had both the highest mean value of $S_{280-500}$ and the lowest mean value of $S_{350-500}$. Increases in the spectral slope of CDOM as a result of photo-bleaching have been reported [20–22]. However, the derived values of $S_{280-500}$ for LN water, are higher than corresponding values for lakes on the Yungui Plateau, where the mean value of $S_{280-500}$ was found to range from 0.0146 to 0.0232 nm^{-1} [37]. Excluding LN, the mean value of $S_{280-500}$ for the other five study sites was found to vary in the range 0.017–0.022 nm^{-1}, and an even narrower range of 0.014–0.015 nm^{-1} was found for $S_{350-500}$ (Table 3).
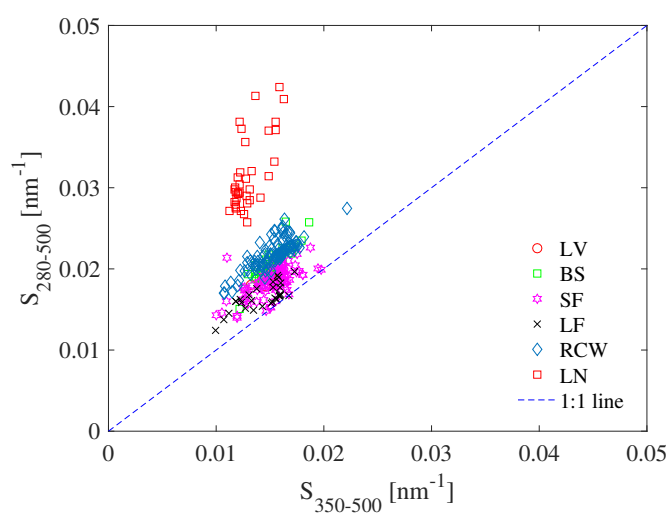

Figure 3. Scatter plots of the CDOM absorption spectral slope derived using nonlinear fitting methods for all study sites for $S_{350-500}$ versus $S_{280-500}$.

For a given water body, the S values tend to be restricted to a narrow range. Bricaud et al. [7] observed that $S_{375-500}$ for oceanic water varied in the range of 0.010–0.020 nm^{-1} with an average value of 0.014 nm^{-1}. For various coastal water bodies around Europe (English Channel, Adriatic, Baltic, Mediterranean, and the North Sea), Babin et al. [10] found $S_{350-500}$ to vary in the range 0.0114–0.0251 nm^{-1} with a mean value of 0.0176 nm^{-1}. From the equatorial to the subarctic Pacific regions, Yamashita and Tanoue [68] found $S_{320-350}$ to vary between 0.017 and 0.036 with a mean value of 0.023 nm^{-1}. Zhang et al. [37] found $S_{280-500}$ to vary in the range 0.0189 ± 0.0094 nm^{-1} for lakes on the Yungui Plateau with altitudes ranging from 1516 to 4591 m.

$S_{350-500}$ values in the range 0.015–0.017 nm^{-1} are typical for the brackish Gulf of Bothnia in the Baltic Sea, while they vary within a wide range (0.013–0.021 nm^{-1}) for the oceanic water of the Baltic proper [69]. According to Green and Blough [70], $S_{290-360}$ values around 0.030 nm^{-1} and $S_{290-500}$ around 0.014 nm^{-1} indicate water of oceanic and terrestrial (i.e., river outlets) origin, respectively. In the Arctic Ocean, $S_{300-600}$ varies between 0.008 and 0.047 nm^{-1}, but in the Eurasian part of the Arctic Ocean and in the Greenland Sea the values are lower, 0.015–0.021 nm^{-1} [61] and 0.016–0.020 nm^{-1} [31], respectively, which are in good agreement with corresponding values for our marine sites (see Table 3), and also compare well with $S_{300-600}$ = 0.017–0.026 nm^{-1} for the northeastern U.S. Atlantic coast [24].

Table 3. The maximum (max), minimum (min), mean, and standard deviation (STD) values for CDOM absorption spectral slopes $S_{280-500}$ and $S_{350-500}$ at each study site.

Location		$S_{280-500}$ [nm^{-1}]	$S_{350-500}$ [nm^{-1}]
Lake Victoria (LV)	Max	0.020	0.015
	Min	0.018	0.013
	Mean	0.019	0.015
	STD	0.001	0.001
Bohai Sea (BS)	Max	0.026	0.019
	Min	0.015	0.012
	Mean	0.021	0.015
	STD	0.002	0.001
Samnangerfjord (SF)	Max	0.023	0.020
	Min	0.014	0.010
	Mean	0.018	0.015
	STD	0.002	0.002
Lysefjord (LF)	Max	0.020	0.017
	Min	0.013	0.010
	Mean	0.017	0.014
	STD	0.002	0.002
Røst Coastal Water (RCW)	Max	0.027	0.022
	Min	0.017	0.011
	Mean	0.022	0.015
	STD	0.002	0.002
Lake Namtso (LN)	Max	0.042	0.016
	Min	0.026	0.011
	Mean	0.032	0.013
	STD	0.005	0.001

For the Kattegat–Skagerrak area (eastern North Sea), mean $S_{250-450}$ values around 0.023 nm^{-1} were found during spring and summer [71]. Closer to the river discharges, as in the Oslo fjord, Højerslev and Aas [71] found the average $S_{250-450}$ value to be 0.0175 nm^{-1}, which is close to the mean $S_{275-425}$ spring value of 0.018 nm^{-1} found for the NCC water off the southern coast of Norway [25]. The mean values of $S_{350-500}$ for our six water bodies, however, were found to be lower than those reported by Babin et al. [10] for coastal water around Europe ($S_{350-500}$ = 0.0176 nm^{-1}), even though the same procedures (i.e., methods for correction of scattering due to residual particles, for fitting, and for choice of wavelength interval for fitting) were followed. The deviation could be due to different CDOM sources, but it should be noted that in the study of Babin et al. [10], the mean value of $S_{350-500}$ for the North Sea site, which is closest to our study sites in Norway, was lower (0.0167 nm^{-1}) than the other mean values in their study. The North Sea values were obtained from 96 samplings conducted during the phytoplankton growth season in April, May, and September, and they compare well with our number of samplings and sampling period.

Plots of $a_{CDOM}(\lambda)$ against S can give information about the CDOM origin. Figure 4a,b show scatter plots of the spectral slopes $S_{350-500}$ and $S_{280-500}$ for each study site versus the CDOM absorption coefficient at 440 nm [$a_{CDOM}(440)$], while Figure 4c,d show scatter plots of the spectral slopes $S_{350-500}$ and $S_{280-500}$ for each study site versus the CDOM absorption coefficient at 320 nm [$a_{CDOM}(320)$]. It can be seen that the degree of linear relationship between the base-10 logarithm of $a_{CDOM}(440)$ or $a_{CDOM}(320)$ and the spectral slope $S_{350-500}$ or $S_{280-500}$ is site dependent. There is a strong negative linear relationship between the base-10 logarithm of $a_{CDOM}(440)$ and either of the spectral slopes $S_{350-500}$ and $S_{280-500}$ for RCW with correlation coefficients r equal to -0.88 and -0.67, respectively. Figure 4b shows that the strongest negative linear relationship between the base-10 logarithm of $a_{CDOM}(440)$ and $S_{280-500}$ was found in LN ($r_{LN} = -0.91$) and the second strongest in LV ($r_{LV} = -0.90$).

Figure 4b,d show that when all study sites were considered, there was a strong negative linear relationship between the base-10 logarithm of $a_{CDOM}(440)$ and the spectral slope $S_{280-500}$ ($r_{all} = -0.76$), as well as between the base-10 logarithm of $a_{CDOM}(320)$ and the spectral slope $S_{280-500}$ ($r_{all} = -0.71$). It also can be seen in Figure 4b,d that the data points for the CDOM samples from RCW, LF, and SF have similar distribution patterns, while the corresponding data points for BS and LV tend to deviate from these patterns in both cases, with a narrow range of $a_{CDOM}(440)$ and $a_{CDOM}(320)$ values shifted towards the upper part of the scale, possibly implying that the composition of the CDOM samples in BS differed from that in the mesotrophic RCW, LF, and SF. Special for the BS near-shore water is the high occurrence of mineral particles, supported by rivers and sediment resuspension by winds and tides [72]. In this context, it is interesting to note that clay particles are found to preferentially adsorb the chromophoric part of dissolved organic carbon, and thereby contribute to its removal from the dissolved fraction [73]. Compared with $a_{CDOM}(443)$ and $S_{350-500}$ data from Babin et al. [10], our value ranges for RCW, LF, and SF compare well with the characteristics given for the North Sea water, including a negative linear relationship. This confirms the strong coupling between Norwegian Coastal Water/Fjord Water and North Sea/Atlantic Water, which is known to be regulated by wind-driven water exchanges [74].

To find out more about the CDOM origin, we have plotted $S_{300-650}$ for all water bodies against $a_{CDOM}(375)$ and included the model curve for mixing of autochthonous CDOM with oceanic CDOM derived by Stedmon and Markager [31] (Figure 4e). It can be seen that the distribution of points follow the pattern depicted by the Stedmon and Markager [31] curve quite well. Data points to the left represent water with low terrestrial inputs (low $a_{CDOM}(375)$ and high $S_{300-650}$ values), while data points to the right represent water with high terrestrial inputs (higher $a_{CDOM}(375)$ and lower $S_{300-650}$ values). In terms of Stedmon and Markager [31] classification of trophic state, water with $a_{CDOM}(375)$ < 0.1 m^{-1} and $S_{300-650}$ > 25 µm^{-1} contains oceanic CDOM, water with $a_{CDOM}(375)$ = 0.5–0.6 m^{-1} and $S_{300-650} \sim 10$ µm^{-1} contains autochthonous CDOM, and water with $a_{CDOM}(375)$ > 0.6 m^{-1} and $S_{300-650}$ = 15–21 µm^{-1} (horizontal lines in Figure 4e) contains terrestrial CDOM. In our case, this means that the mesotrophic fjord water bodies (LF and SF), the eutrophic lake water (LV), and the coastal marine water (BS) are mainly dominated by terrestrial inputs, but with some contribution of autochthonous CDOM, and with BS being more influenced by terrestrial discharges than LF and SF. The mesotrophic coastal–oceanic Norwegian water (RCW), on the other hand, is less influenced by terrestrial CDOM, but more by a mixture of autochthonous and oceanic CDOM. Interestingly, the oligotrophic LN has CDOM characteristics resembling those of "oceanic"-autochthonous origin, implying a dominance of decomposed and low molecular CDOM.
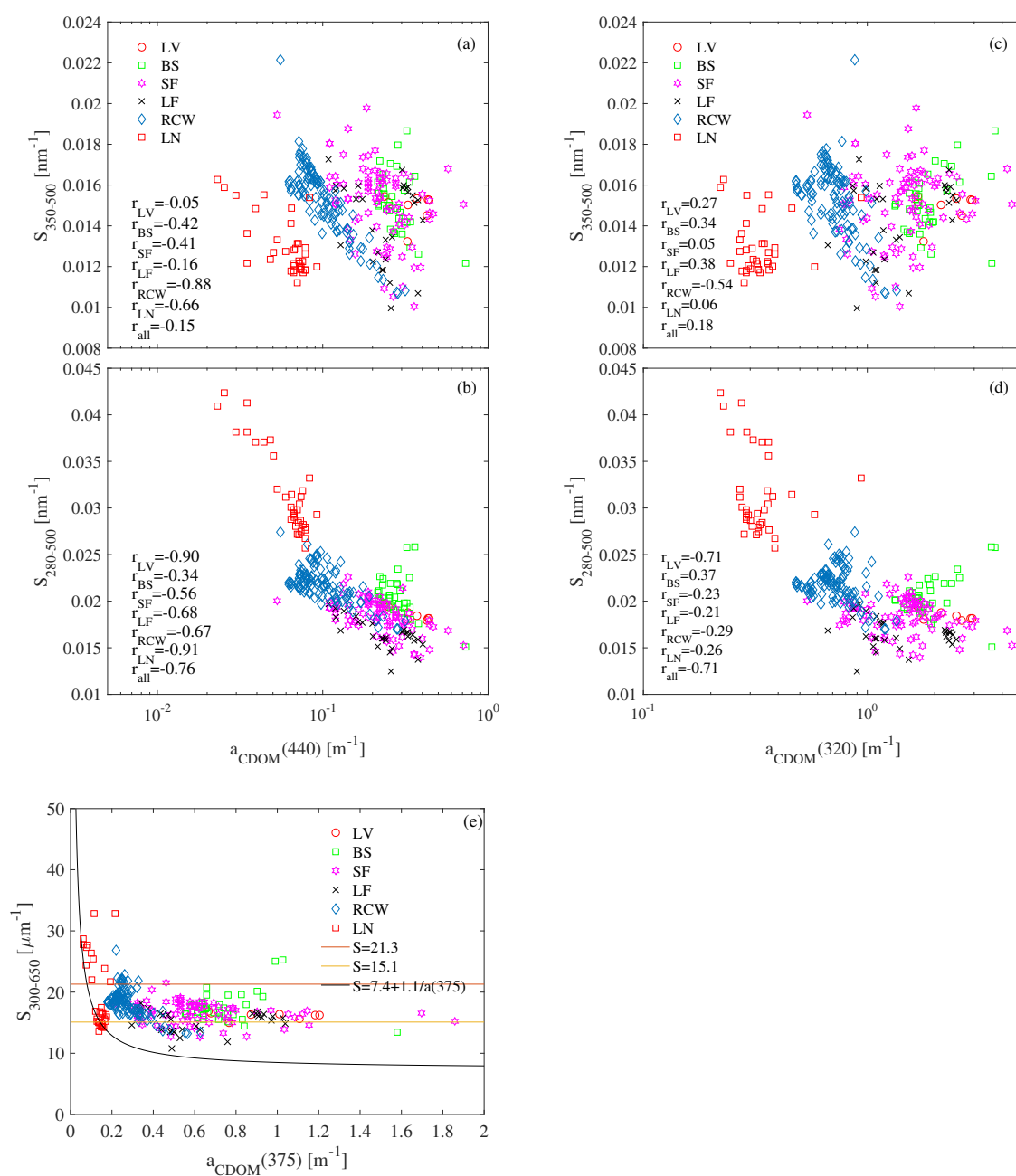
Figure 4. Scatter plots of (**a**) $S_{350-500}$ and (**b**) $S_{280-500}$ for all six study sites versus the CDOM absorption coefficient at 440 [$a_{CDOM}(440)$]. Scatter plots of (**c**) $S_{350-500}$ and (**d**) $S_{280-500}$ for all six study sites versus the CDOM absorption coefficient at 320 [$a_{CDOM}(320)$]. r is the correlation coefficient between $S_{350-500}$ or $S_{280-500}$ and the natural logarithm of $a_{CDOM}(440)$ or $a_{CDOM}(320)$ for each study site as specified by the subscript. r_{all} is the correlation coefficient for all study sites. (**e**) Scatter plots of the CDOM absorption spectral slope $S_{300-650}$ for all study sites versus the CDOM absorption coefficient at 375 [$a_{CDOM}(375)$]. Black curve is drawn after Stedmon and Markager [31].

3.3. $S_{280-295}$ / $S_{350-400}$ Ratios Used as Indicators of CDOM Photobleaching

To investigate possible effects of UV exposure on spectral CDOM absorption characteristics for different water bodies in this study, we calculated the ratio S_R of $S_{280-295}$ to $S_{350-400}$. According to Coble [75], only compounds absorbing below 300 nm could resist prolonged exposure in surface water, and Helms et al. [26] showed that both $S_{275-295}$ and $S_R = S_{275-295}/S_{350-400}$ ratios are inversely related to the molecular weight of CDOM. Figure 5 shows the $S_{280-295}/S_{350-400}$ ratio (we did not have CDOM

absorption coefficient data below 280 nm) plotted against $a_{\mathrm{CDOM}}(440)$. The deviation of the data points for LN from those for the other water bodies, is probably due to photo-bleaching of CDOM. The high S_{R} values (2.2–4.2) and low $a_{\mathrm{CDOM}}(440)$ values (0.025–0.08 [m^{-1}]) are indicative of decomposed humic-like substances, and the formation of low molecular compounds, due to strong solar irradiance at high altitudes [34]. With the exception of five outliers, four from SF and one from BS, all the other water bodies had values within the S_{R} range 1–2.25, with corresponding $a_{\mathrm{CDOM}}(440)$ values within the range 0.05–0.45 [m^{-1}]. It should be noted that the highly polluted and eutrophic LV had values within narrow ranges, whereas the SF was characterized by larger $a_{\mathrm{CDOM}}(440)$ variations. The fact that the BS data group closely together with values for other marine sites, such as LF and SF, but less closely with values for RCW, could be due to impacts of freshwater discharges, containing clay/mineral particles. RCW is dominated by coastal-oceanic water with lower content of terrestrial DOM [1]. If we ignore the five outliers, another interesting feature of our data is that there is no S_{R} value <1, which means that $S_{280-295} \geq S_{350-400}$, and therefore there is an excess of low molecular weight CDOM at all sites. Also, RCW, BS, and, LV are more impacted by decomposed compounds, with mean values around 1.7, than the Norwegian fjords, where the water is close to its CDOM sources, and therefore less decomposed (i.e., more high molecular compounds) than farther out in the open ocean.
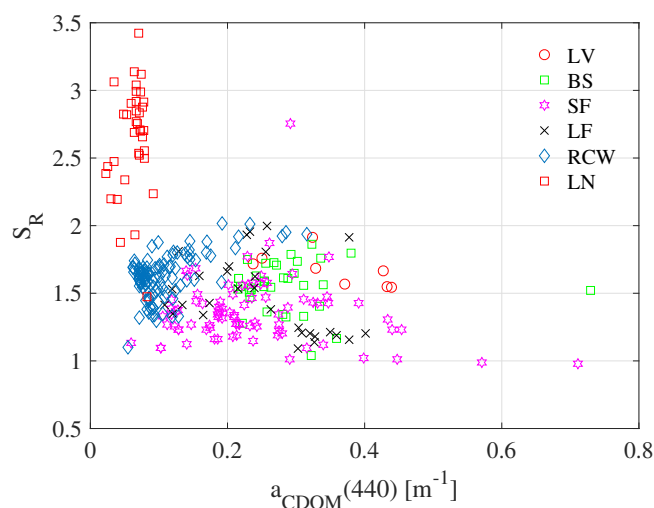

Figure 5. Scatter plot of $S_R(S_{280-295}/S_{350-400})$ versus the CDOM absorption coefficient at 440 [$a_{\mathrm{CDOM}}(440)$].

For the Chesapeake Bay river-estuary system, S_{R} varies within the range 0.72–2.52 [26], which compares well with our data for BS, LV, LF, and SF. The surprisingly high similarities in S_{R} values for the BS, LV, LF, and SF water bodies (Figure 5), despite large differences in trophic state, could be due to their content of suspended particulate matter, which may contribute to scattering of incoming UV light, and thereby to reduced photobleaching of humic-like substances (CDOM). The fact that LV had about 10 times larger Chl-*a* concentrations than BS, LF, and SF (Table 1), indicates that scattering by phytoplankton cell cover/walls and absorption by pigments were of minor importance in this context. Like BS, also LF and SF are supported by inorganic clay (<0.002 mm) and silt (0.063–0.002 mm) particles during the snow melting period [72,76].

It should be emphasized that more information on S_{R} versus $a_{\mathrm{CDOM}}(440)$ relationships for different water types is a prerequisite for development of algorithms for accurate retrieval of CDOM absorption and photobleaching from space. Unfortunately, so far there is no operational satellite color sensor with spectral absorption lower than 412 nm available for monitoring the upper layer of the ocean [27], but efforts are being made to include UV wavelengths in the next generation of ocean color sensors [24,27]. Also, for analysis of historical ocean color data for different water bodies, improved knowledge on CDOM absorption characteristics is vital, since site specific *S* plots can be

used to extrapolate satellite retrieved CDOM absorption into the UV spectral region. We hope our data can contribute constructively in this context.

4. Conclusions

In our data set, which covers six different geographical regions, the mean CDOM absorption coefficients at 320 nm and 440 nm were found to vary in the ranges 0.34–2.28 m^{-1} and 0.063–0.35 m^{-1}, respectively. The highest mean value was found in LV and the lowest mean value in LN. Next to LN was RCW and next to LV was BS, while the fjord water bodies LF and SF were situated in between these two extreme groups. Our results indicate that for a water body it is important to specify the spectral range for which the spectral slope S is estimated, and that care should be taken when comparing S values in the literature, which are derived for different wavelength ranges. Thus, the mean spectral slopes $S_{280-500}$ and $S_{350-500}$ were found to vary in the ranges of 0.017–0.032 nm^{-1} and 0.013–0.015 nm^{-1}, respectively. The highest mean value for $S_{280-500}$ as well as the lowest mean value for $S_{350-500}$ were found in LN. Considering all study sites, we found a strong negative linear relationship between the base-10 logarithm of $a_{\text{CDOM}}(440)$ and the spectral slope $S_{280-500}$, and also between the base-10 logarithm of $a_{\text{CDOM}}(320)$ and the spectral slope $S_{280-500}$. Scatter plots of $S_{280-500}$ versus $a_{\text{CDOM}}(440)$ and $a_{\text{CDOM}}(320)$ revealed a close connection between RCW, LF, and SF on one side, and between BS and LV on the other side. CDOM seems to originate from terrestrial sources in LF, SF, BS, and LV, while RCW is characterized by autochthonous-oceanic CDOM, and LN by autochthonous CDOM. Photobleaching of CDOM is prominent in LN, indicated by reduced absorption towards short wavelengths in the UV spectrum, resulting in very high $S_{280-500}$ values and low $a_{\text{CDOM}}(320)$ values. For the other water bodies, only modest photobleaching was found. We conclude that high altitudes, implying high UV radiation levels, and oligotrophic water conditions are important to make a significant change in CDOM absorption properties.

Author Contributions: Data curation, C.N.; formal analysis, C.N. and S.R.E.; funding acquisition, J.J.S. and D.L.; investigation, C.N., B.H., J.J.S., Y.-C.C., K.S., M.N., Q.X., D.M., T.S. and K.H.S.; supervision, Ø.F. and J.J.S.; writing—original draft, C.N. and S.R.E.

Conflicts of Interest: The authors declare no conflict of interest.

References

1. Kirk, J.T.O. *Light and Photosynthesis in Aquatic Ecosystems*, 3rd ed.; Cambridge University Press: Cambridge, UK, 2011; pp. 1–3.
2. Bowers, D.G.; Evans, D.; Thomas, D.N.; Ellis, K.M.; Williams, P.J.L.B. Interpreting the colour of an estuary. *Estuar. Coast. Shelf Sci.* **2004**, *59*, 13–20. [CrossRef]
3. Warnock, R.E.; Gieskes, W.W.C.; Van Laar, S. Regional and seasonal differences in light absorption by yellow substance in the Southern Bight of the North Sea. *J. Sea Res.* **1999**, *42*, 169–178. [CrossRef]
4. Kalle, K. Meereskundliche chemische Untersuchungen mit Hilfe des Zeißchen Pulfrich-Photometers, VI. Mitt., Die Bestimmung des Nitrats und des Gelbstoffes (in German). *Ann. Hydrogr. Maritim. Meteorol.* **1937**, *65*, 276–282.
5. Shank, G.C.; Zepp, R.G.; Vähätalo, A.; Lee, R.; Bartels, E. Photobleaching kinetics of chromophoric dissolved organic matter derived from mangrove leaf litter and floating Sargassum colonies. *Mar. Chem.* **2010**, *119*, 162–171. [CrossRef]
6. Steinberg, D.K.; Nelson, N.B.; Carlson, C.A.; Prusak, A.C. Production of chromophoric dissolved organic matter (CDOM) in the open ocean by zooplankton and the colonial cyanobacterium *Trichodesmium* spp. *Mar. Ecol. Prog. Ser.* **2004**, *267*, 45–56. [CrossRef]

7.　Bricaud, A.; Morel, A.; Prieur, L. Absorption by dissolved organic matter of the sea (yellow substance) in the UV and visible domains. *Limnol. Oceanogr.* **1981**, *26*, 43–53. [CrossRef]

8.　Stedmon, C.A.; Markager, S.; Kaas, H. Optical properties and signatures of chromophoric dissolved organic matter (CDOM) in Danish coastal waters. *Estuar. Coast. Shelf Sci.* **2000**, *51*, 267–278. [CrossRef]

9.　Nelson, N.B.; Siegel, D.A. The global distribution and dynamics of chromophoric dissolved organic matter. *Annu. Rev. Mar. Sci.* **2013**, *5*, 447–476. [CrossRef]

10.　Babin, M.; Stramski, D.; Ferrari, G.M.; Claustre, H.; Bricaud, A.; Obolensky, G.; Hoepffner, N. Variations in the light absorption coefficients of phytoplankton, nonalgal particles, and dissolved organic matter in coastal waters around Europe. *J. Geophys. Res.* **2003**, *108*, 4.1–4.20. [CrossRef]

11.　Frette, Ø.; Erga, S.R.; Hamre, B.; Aure, J.; Stamnes, J.J. Seasonal variability in inherent optical properties in a western Norwegian fjord. *Sarsia* **2004**, *89*, 276–291. [CrossRef]

12.　Castillo, C.E.D.; Coble, P.G. Seasonal variability of the colored dissolved organic matter during the 1994–95 NE and SW Monsoons in the Arabian Sea. *Deep Sea Res. Part II Top. Stud. Oceanogr.* **2000**, *47*, 1563–1579. [CrossRef]

13.　Kowalczuk, P. Seasonal variability of yellow substance absorption in the surface layer of the Baltic Sea. *J. Geophys. Res.* **1999**, *104*, 30047–30058. [CrossRef]

14.　Matsuoka, A.; Hooker, S.B.; Bricaud, A.; Gentili, B.; Babin, M. Estimating absorption coefficients of colored dissolved organic matter (CDOM) using a semi-analytical algorithm for southern Beaufort Sea waters: applications to deriving concentrations of dissolved organic carbon from space. *Biogeosciences* **2013**, *10*, 917–927. [CrossRef]

15.　Shang, Y.; Song, K.; Wen, Z.; Lyu, L.; Zhao, Y.; Fang, C.; Zhang, B. Characterization of CDOM absorption of reservoirs with its linkage of regions and ages across China. *Environ. Sci. Pollut. Res.* **2018**, *25*, 16009–16023. [CrossRef]

16.　Massicotte, P.; Asmala, E.; Stedmon, C.A.; Markager, S. Global distribution of dissolved organic matter along the aquatic continuum: Across rivers, lakes and oceans. *Sci. Total Environ.* **2017**, *609*, 180–191. [CrossRef]

17.　Ogawa, H.; Tanoue, E. Dissolved Organic Matter in Oceanic Waters. *J. Oceanogr.* **2003**, *59*, 129–147. [CrossRef]

18.　Blumthaler, M.; Ambach, W.; Rehwald, W. Solar UV-A and UV-B radiation fluxes at two alpine stations at different altitudes. *Theor. Appl. Climatol.* **1992**, *46*, 39–44. [CrossRef]

19.　Alexandris, D.; Varotsos, C.; Ya Kondratyev, K.; Chronopoulos, G. On the altitude dependence of solar effective UV. *Phys. Chem. Earth Part C* **1999**, *24*, 515–517. [CrossRef]

20.　Brinkmann, T.; Sartorius, D.; Frimmel, F.H. Photobleaching of humic rich dissolved organic matter. *Aquat. Sci.* **2003**, *65*, 415–424. [CrossRef]

21.　Del Vecchio, R.; Blough, N.V. Photobleaching of chromophoric dissolved organic matter in natural waters: Kinetics and modeling. *Mar. Chem.* **2002**, *78*, 231–253. [CrossRef]

22.　Twardowski, M.S.; Donaghay, P.L. Photobleaching of aquatic dissolved materials: Absorption removal, spectral alteration, and their interrelationship. *J. Geophys. Res.* **2002**, *107*, C8. [CrossRef]

23.　Arrigo, K.R.; Brown, C.W. Impact of chromophoric dissolved organic matter on UV inhibition of primary productivity in the sea. *Mar. Ecol. Prog. Ser.* **1996**, *140*, 207–216. [CrossRef]

24.　Mannino, A.; Novak, M.G.; Hooker, S.B.; Hyde, K.; Aurin, D. Algorithm development and validation of CDOM properties for estuarine and continental shelf waters along the northeastern U.S. coast. *Remote Sens. Environ.* **2014**, *152*, 576–602. [CrossRef]

25.　Erga, S.; Aursland, K.; Frette, Ø.; Hamre, B.; Lotsberg, J.; Stamnes, J.; Aure, J.; Rey, F.; Stamnes, K. UV transmission in Norwegian marine waters: Controlling factors and possible effects on primary production and vertical distribution of phytoplankton. *Mar. Ecol. Prog. Ser.* **2005**, *305*, 79–100. [CrossRef]

26.　Helms, J.R.; Stubbins, A.; Ritchie, J.D.; Minor, E.C.; Kieber, D.J.; Mopper, K. Absorption spectral slopes and slope ratios as indicators of molecular weight, source, and photobleaching of chromophoric dissolved organic matter. *Limnol. Oceanogr.* **2008**, *53*, 955–969. [CrossRef]

27.　Wei, J.; Lee, Z.; Ondrusek, M.; Mannino, A.; Tzortziou, M.; Armstrong, R.A. Spectral slopes of the absorption coefficient of colored dissolved and detrital material inverted from UV-visible remote sensing reflectance. *J. Geophys. Res. Ocean.* **2016**, *121*, 1953–1969. [CrossRef]

28. Blough, N.V.; Del Vecchio, R. Chromophoric DOM in the coastal environment. In *Biogeochemistry of Marine Dissolved Organic Matter*; Hansell, D.A., Carlson, C.A., Eds.; Academic Press: San Diego, CA, USA, 2002; pp. 509–546.

29. Conmy, R.N.; Coble, P.G.; Chen, R.F.; Gardner, G.B. Optical properties of colored dissolved organic matter in the Northern Gulf of Mexico. *Mar. Chem.* **2004**, *89*, 127–144. [CrossRef]

30. Matsuoka, A.; Ortega-Retuerta, E.; Bricaud, A.; Arrigo, K.R.; Babin, M. Characteristics of colored dissolved organic matter (CDOM) in the Western Arctic Ocean: Relationships with microbial activities. *Deep-Sea Res. Part II* **2015**, *118*, 44–52. [CrossRef]

31. Stedmon, C.A.; Markager, S. The optics of chromophoric dissolved organic matter (CDOM) in the Greenland Sea: An algorithm for differentiation between marine and terrestrially derived organic matter. *Limnol. Oceanogr.* **2001**, *46*, 2087–2093. [CrossRef]

32. Matsuoka, A.; Hill, V.; Huot, Y.; Babin, M.; Bricaud, A. Seasonal variability in the light absorption properties of western Arctic waters: Parameterization of the individual components of absorption for ocean color applications. *J. Geophys. Res.* **2011**, *116*, C02007. [CrossRef]

33. Vodacek, A.; Blough, N.V.; DeGrandpre, M.D.; Nelson, R.K. Seasonal variation of CDOM and DOC in the Middle Atlantic Bight: Terrestrial inputs and photooxidation. *Limnol. Oceanogr.* **1997**, *42*, 674–686. [CrossRef]

34. Song, K.; Shang, Y.; Wen, Z.; Jacinthe, P.; Liu, G.; Lyu, L.; Fang, C. Characterization of CDOM in saline and freshwater lakes across China using spectroscopic analysis. *Water Res.* **2019**, *150*, 403–417. [CrossRef]

35. Okullo, W.; Ssenyonga, T.; Hamre, B.; Frette, Ø.; Sørensen, K.; Stamnes, J.J.; Steigen, A.; Stamnes, K. Parameterization of the inherent optical properties of Murchison Bay, Lake Victoria. *Appl. Opt.* **2007**, *46*, 8553–8561. [CrossRef]

36. Twardowski, M.S.; Boss, E.; Sullivan, J.M.; Donaghay, P.L. Modeling the spectral shape of absorption by chromophoric dissolved organic matter. *Mar. Chem.* **2004**, *89*, 69–88. [CrossRef]

37. Zhang, Y.L.; Zhang, E.L.; Yin, Y.; Van Dijk, M.A.; Feng, L.Q.; Shi, Z.Q.; Liu, M.L.; Qin, B.Q. Characteristics and sources of chromophoric dissolved organic matter in lakes of the Yungui Plateau, China, differing in trophic state and altitude. *Limnol. Oceanogr.* **2010**, *55*, 2645–2659. [CrossRef]

38. The Encyclopedia of Earth: Lake Victoria. Available online: http://www.eoearth.org/view/article/154134/ (accessed on 7 February 2015).

39. Dorji, T.; Totland, Ø.; Moe, S.R.; Hopping, K.A.; Pan, J.B.; Klein, J.A. Plant functional traits mediate reproductive phenology and success in response to experimental warming and snow addition in Tibet. *Glob. Chang. Biol.* **2013**, *19*, 459–472. [CrossRef]

40. Kang, S.C.; Yang, Y.P.; Zhu, L.P.; Ma, Y.M. *Modern Environmental Processes and Changes in the Nam Co basin, Tibetan Plateau*; Meteorological Press: Beijing, China, 2011; pp. 16–22.

41. Norsang, G.; Chen, Y.C.; Pingcuo, N.; Dahlback, A.; Frette, Ø.; Kjeldstad, B.; Hamre, B.; Stamnes, K.; Stamnes, J.J. Comparison of ground-based measurements of solar UV radiation at four sites on the Tibetan Plateau. *Appl. Opt.* **2014**, *53*, 736–747. [CrossRef]

42. Ssebiyonga, N.; Erga, S.R.; Hamre, B.; Stamnes, J.J.; Frette, O. Light conditions and photosynthetic efficiency of phytoplankton in Murchison Bay, Lake Victoria, Uganda. *Limnologica* **2013**, *43*, 185–193. [CrossRef]

43. Erga, S.R.; Ssebiyonga, N.; Frette, Ø.; Hamre, B.; Aure, J.; Strand, Ø.; Strohmeier, T. Dynamics of phytoplankton distribution and photosynthetic capacity in a western Norwegian fjord during coastal upwelling: Effects on optical properties. *Estuar. Coast. Shelf Sci.* **2012**, *97*, 91–103. [CrossRef]

44. Röhrs, J.; Kai, H.C.; Vikebø, F.; Sundby, S.; Saetra, Ø.; Broström, G. Wave-induced transport and vertical mixing of pelagic eggs and larvae. *Limnol. Oceanogr.* **2014**, *59*, 1213–1227.

45. Nima, C.; Hamre, B.; Frette, Ø.; Erga, S.R.; Chen, Y.C.; Zhao, L.; Sørensen, K.; Norli, M.; Lu, D.R.; Xing, Q.G.; et al. Impact of particulate and dissolved material on light absorption properties in a High-Altitude Lake in Tibet, China. *Hydrobiologia* **2016**, *768*, 63–79. [CrossRef]

46. Nima, C.; Frette, O.; Hamre, B.; Erga, S.R.; Chen, Y.; Zhao, L.; Sorensen, K.; Norli, M.; Stamnes, K.; Stamnes, J.J. Absorption properties of high-latitude Norwegian coastal water: The impact of CDOM and particulate matter. *Estuar. Coast. Shelf Sci.* **2016**, *178*, 158–167. [CrossRef]

47. Erga, S.R.; Ssebiyonga, N.; Hamre, B.; Frette, Ø.; Hovland, E.K.; Hancke, K.; Drinkwater, K.F.; Rey, F.E.D. Environmental control of phytoplankton distribution and photosynthetic performance at the Jan Mayen Front in the Norwegian Sea. *J. Mar. Syst.* **2014**, *130*, 193–205. [CrossRef]

48. Boyd, T.J.; Osburn, C.L. Changes in CDOM fluorescence from allochthonous and autochthonous sources during tidal mixing and bacterial degradation in two coastal estuaries. *Mar. Chem.* **2004**, *89*, 189–210. [CrossRef]

49. Retamal, L.; Vincent, W.F.; Martineau, C.; Osburn, C.L. Comparison of the optical properties of dissolved organic matter in two river-influenced coastal regions of the Canadian Arctic. *Estuar. Coast. Shelf Sci.* **2007**, *72*, 261–272. [CrossRef]

50. Granskog, M.A.; Macdonald, R.W.; Mundy, C.J.; Barber, D.G. Distribution, characteristics and potential impacts of chromophoric dissolved organic matter (CDOM) in Hudson Strait and Hudson Bay, Canada. *Cont. Shelf Res.* **2007**, *27*, 2032–2050. [CrossRef]

51. Holmes, R.W. The secchi disk in turbid coastal waters1. *Limnol. Oceanogr.* **1970**, *15*, 688–694. [CrossRef]

52. Eilertsen, H.C.; Frantzen, S. Phytoplankton from two sub-Arctic fjords in northern Norway 2002–2004: I. Seasonal variations in chlorophyll a and bloom dynamics. *Mar. Biol. Res.* **2007**, *3*, 319–332. [CrossRef]

53. Norsang, G.; Kocbach, L.; Wangmu, T.; Stamnes, J.J.; Dahlback, A.; Pingcuo, N. Ground-based measurements and modeling of solar UV-B radiation in Lhasa, Tibet. *J. Atmos. Environ.* **2009**, *43*, 1498–1502. [CrossRef]

54. Norsang, G.; Kocbach, L.; Stamnes, J.J.; Wangmu, T.; Pingcuo, N. Spatial distribution and temporal variation of solar UV radiation over the Tibetan Plateau. *Appl. Phys. Res.* **2011**, *3*, 37–46. [CrossRef]

55. Carvalho, S.I.M.; Otero, M.; Duarte, A.C.; Santos, E.B.H. Spectroscopic changes on fulvic acids from a kraft pulp mill effluent caused by sun irradiation. *Chemosphere* **2008**, *73*, 1845–1852. [CrossRef]

56. Carreto, J.I.; Carignan, M.O.; Montoya, N.G. A high-resolution reverse-phase liquid chromatography method for the analysis of mycosporine-like amino acids (MAAs) in marine organisms. *Mar. Biol.* **2005**, *146*, 237–252. [CrossRef]

57. Tilstone, G.H.; Airs, R.L.; Vicente, V.M.; Widdicombe, C.E.; Llewellyn, C.A. High concentrations of mycosporine-like amino acids and colored dissolved organic matter in the sea surface microlayer off the Iberian Peninsula. *Limnol. Oceanogr.* **2010**, *55*, 1835–1850. [CrossRef]

58. Pavlov, A.K.; Silyakova, A.; Granskog, M.A.; Bellerby, R.G.J.; Engel, A.; Schulz, K.G.; Brussaard, C.P.D. Marine CDOM accumulation during a coastal Arctic mesocosm experiment: No response to elevated pCO2 levels. *J. Geophys. Res. Biogeosci.* **2014**, *119*, 1216–1230. [CrossRef]

59. Li, S.; Zhang, J.; Mu, G.; Ju, H.; Wang, R.; Li, D.; Shabbir, A.H. Spatiotemporal Characterization of Chromophoric Dissolved Organic Matter (CDOM) and CDOM-DOC Relationships for Highly Polluted Rivers. *Water* **2016**, *8*, 399. [CrossRef]

60. Shao, T.; Zheng, H.; Song, K.; Zhao, Y.; Zhang, B. Influence of environmental factors on absorption characteristics of suspended particulate matter and CDOM in Liaohe River watershed, northeast China. *Environ. Sci. Pollut. Res.* **2017**, *24*, 19322–19337. [CrossRef]

61. Stedmon, C.A.; Amon, R.M.W.; Rinehart, A.J.; Walker, S.A. The supply and characteristics of colored dissolved organic matter (CDOM) in the Arctic Ocean: Pan Arctic trends and differences. *Mar. Chem.* **2011**, *124*, 108–118. [CrossRef]

62. Chen, C. Chemical and physical fronts in the Bohai, Yellow and East China seas. *J. Mar. Syst.* **2009**, *78*, 394–410. [CrossRef]

63. Aksnes, D.L.; Dupont, N.; Staby, A.; Fiksen, .; Kaartvedt, S.; Aure, J. Coastal water darkening and implications for mesopelagic regime shifts in Norwegian fjords. *Mar. Ecol. Prog. Ser.* **2009**, *387*, 39–49. [CrossRef]

64. Zhang, Y.L.; Zhang, E.L.; Liu, M.L. Spectral absorption properties of chromophoric dissolved organic matter and particulate matter in Yunnan Plateau lakes. *J. Lake Sci.* **2009**, *21*, 255–263. (In Chinese)

65. Chen, B.; Wei, H.; Ma, S.; Feng, M.; Liu, C.; Gu, X.; Kaining, C. Characterization of Chromophoric Dissolved Organic Matter in the Littoral Zones of Eutrophic Lakes Taihu and Hongze during the Algal Bloom Season. *Water* **2018**, *10*, 861. [CrossRef]

66. Meler, J.; Kowalczuk, P.; Ostrowska, M.; Ficek, D.; Zablocka, M.; Zdun, A. Parameterization of the light absorption properties of chromophoricdissolved organic matter in the Baltic Sea and Pomeranian lakes. *Ocean Sci.* **2016**, *12*, 1013–1032. [CrossRef]

67. Zhou, X.J.; Li, W.L.; Chen, L.X.; Liu, Y. Study on ozone change over the Tibetan Plateau. *Acta Meteorol. Sinica* **2006**, *20*, 129–143.

68. Yamashita, Y.; Tanoue, E. Basin scale distribution of chromophoric dissolved organic matter in the Pacific Ocean. *Limnol. Oceanogr.* **2009**, *54*, 598–609. [CrossRef]

69. Harvey, E.T.; Kratzer, S.; Andersson, A. Relationships between colored dissolved organic matter and dissolved organic carbon in different coastal gradients of the Baltic Sea. *Ambio* **2015**, *44*, 392–401. [CrossRef]

70. Green, S.A.; Blough, N.V. Optical absorption and fluorescence properties of chromophoric dissolved organic matter in natural waters. *Limnol. Oceanogr.* **1994**, *39*, 1903–1916. [CrossRef]

71. Højerslev, N.K.; Aas, E. Spectral light absorption by yellow substance in the Kattegat-Skagerrak area. *Oceanologia* **2001**, *43*, 39–60.

72. Qiu, Z.; Sun, D.; Hu, C.; Wang, S.; Zheng, L.; Huan, Y.; Peng, T. Variability of Particle Size Distributions in the Bohai Sea and the Yellow Sea. *Remote Sens.* **2016**, *8*, 949. [CrossRef]

73. Tietjen, T.E.; Vahatalo, A.V.; Wetzel, R.G. Effects of clay mineral turbidity on dissolved organic carbon and bacterial production. *Aquat. Sci.* **2005**, *67*, 51–60. [CrossRef]

74. Erga, S.R.; Haugen, S.B.; Bratbak, G.; Egge, J.K.; Heldal, M.; Mork, K.A.; Norland, S. Seasonal variations in C:N:Si:Ca:P:Mg:S:K:Fe relationships of seston from Norwegian coastal water: Impact of extreme offshore forcing during winter-spring 2010. *Mar. Chem.* **2017**, *196*, 1–12. [CrossRef]

75. Coble, P.G. Marine optical biogeochemistry: The chemistry of ocean color. *Chem. Rev.* **2007**, *107*, 402–418. [CrossRef]

76. Klitgaardkristensen, D.; Buhlmortensen, L. Benthic foraminifera along an offshore-fjord gradient: A comparison with amphipods and molluscs. *J. Nat. Hist.* **1999**, *33*, 317–350. [CrossRef]